SSC-202

The Superconducting Super Collider

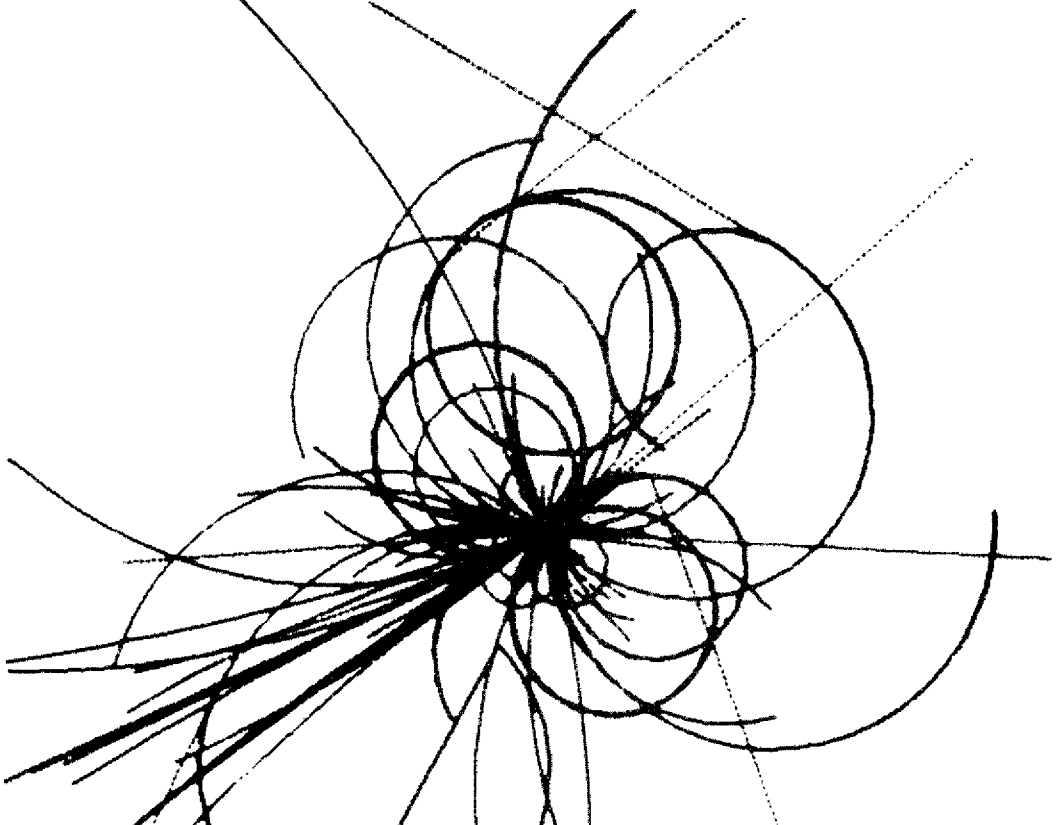

Requirements for Calorimetric Jet Mass Reconstruction for High $p_\perp$ Jets at the SSC

A. Bay and E.M. Wang
Lawrence Berkeley Laboratory
and
D. Bintinger, M.G.D. Gilchriese,
and D.E. Groom
SSC Central Design Group

January 1989

Erratum for SSC-202

Requirements for Calorimetric Jet Mass Reconstruction
for High $p_\perp$ Jets at the SSC

1. Third page, left column, second paragraph, twelth line, add "+0.01" after "$0.15/\sqrt{E}$."
2. Third page, right column, sixteenth line, "$r_{\text{inner}} = 180$ cm" should read "$r_{\text{inner}} = 160$ cm."
3. Fourth page, Table 1, case 2(b) should read

2(b)	78.0	78.6	79.9	80.9
	(5.8)	(6.2)	(6.8)	(10.1)

4. Sixth page, caption for Fig. 3, last line, "Ref. 6" should read "Ref. 3."
5. Sixth page, legend in Fig. 4, add 1 to all reference numbers, e.g. "Ref. 2" should read "Ref. 3."

SSC-202

REQUIREMENTS FOR CALORIMETRIC JET MASS RECONSTRUCTION FOR HIGH $p_\perp$ JETS AT THE SSC

A. Bay and E. M. Wang*

Lawrence Berkeley Laboratory
Berkeley, CA 94720

D. Bintinger, M. G. D. Gilchriese, and D. E. Groom

SSC Central Design Group†
Lawrence Berkeley Laboratory
Berkeley, CA 94720

January 1989

* This work was supported by the Director, Office of Energy Research, Office of High Energy and Nuclear Physics, Division of High Energy Physics of the U.S. Department of Energy, under Contract DE-AC03-76SF00098.

† Operated by the Universities Research Association, Inc. for the Department of Energy.

REQUIREMENTS FOR CALORIMETRIC JET MASS RECONSTRUCTION FOR HIGH $p_\perp$ JETS AT THE SSC

A. Bay and E. M. Wang*
Lawrence Berkeley Laboratory, Berkeley CA 94720

D. Bintinger, M. G. D. Gilchriese, and D. E. Groom
SSC Central Design Group†
Lawrence Berkeley Laboratory, Berkeley CA 94720

Abstract

We have studied two aspects of calorimetry for high $p_\perp$ jets at the SSC. First, the impact of shower containment on very high $p_\perp$ jets and quark compositeness has been studied. Second, the effect of calorimeter granularity on the mass reconstruction of a high $p_\perp$ W ($p_\perp > 500$ GeV/c) producing jets has been examined in detail. We conclude, based on possible compositeness signatures only, that shower leakage has little effect on the compositeness signal for a calorimeter thickness greater than about eight absorption lengths. Mass resolution of very high $p_\perp$ W's reconstructed from hadronic decays of the W is strongly affected by intrinsic shower spreading as well as calorimeter granularity. These effects are quantified.

1. Introduction

Many previous SSC studies have used, as a simple calorimeter simulation, 4-vectors binned in rapidity and azimuth. At some level, energy smearing was applied to simulate effects of calorimeter resolution. In a real calorimeter, however, a given incoming hadron deposits its energy spatially as a shower of electromagnetic and hadronic particles. Some of this energy may even leak out of the calorimeter or be absorbed by inactive material (supports, cryostat walls, etc.) We have developed a more realistic calorimeter simulation program and have used it to revisit some aspects of high $p_\perp$ jets and calorimeter requirements for the SSC.

2. Parameterization and validation

The desire for a more realistic treatment of calorimeter response other than binned 4-vectors is satisfied, to some extent, by the use of parameterizations of the average behavior of electromagnetic (EM) and hadronic showers. Average EM and hadronic shower shapes are parameterized and factored into independent pieces, a longitudinal distribution along the particle direction and a transverse distribution perpendicular to the particle direction.

2.1 EM shower parameterization

The EM shower parameterization is given by [1]:

$$\frac{dE}{dz} = k_\parallel \left(\frac{z}{X_0}\right)^{a-1} e^{-bz/X_0}$$

where

$$\begin{aligned} b &= 0.5 \\ a &= b \log\left(\frac{E}{E_{\text{critical}}}\right) \\ z &= \text{longitudinal distance} \\ X_0 &= \text{radiation length} \\ E &= \text{incident particle energy} \\ E_{\text{critical}} &= \frac{0.55}{Z}\ [\text{GeV}] \\ Z &= \text{atomic number} \\ k_\parallel &= \text{normalization constant} \end{aligned}$$

A comparison of data and our longitudinal parameterization is shown in Fig. 1 [2].

The lateral EM shower shape (shown in Fig. 2) is parameterized by a sum of 2 gaussians:

$$\frac{dE}{dr} = k_\perp \left[e^{(-r/\sigma_1)^2} + e^{(-r/\sigma_2)^2}\right]$$

where

$$\begin{aligned} \sigma_1 &= 0.12\ r_{\text{moliere}} \\ \sigma_2 &= 0.80\ r_{\text{moliere}} \\ k_\perp &= \text{normalization constant} \end{aligned}$$

The Moliere radius, r_{moliere}, is the average transverse deflection of an electron with energy equal to the critical energy after travelling one radiation length longitudinally.

2.2 Hadronic shower parameterization

The longitudinal hadronic shower parameterization we have chosen [3] is:

$$\frac{dE}{dz} = c_\parallel \left[w\left(\frac{z}{X_0}\right)^{a-1} e^{-bz/X_0} + (1-w)\left(\frac{z}{\lambda}\right)^{c-1} e^{-dz/\lambda}\right]$$

where

$$\begin{aligned} z &= \text{longitudinal distance} \\ X_0 &= \text{radiation length} \\ \lambda &= \text{absorption length} \\ a, b, c, d, w &= \text{fitted constants} \\ c_\parallel &= \text{normalization constant} \end{aligned}$$

This parameterization has two terms, the first accounting for electromagnetic energy deposition and the second

* This work was supported by the Director, Office of Energy Research, Office of High Energy and Nuclear Physics, Division of High Energy Physics of the U.S. Department of Energy, Contract DE-AC03-76SF00098.

† Operated by the Universities Research Association for the U. S. Department of Energy.

for hadronic energy deposition. References 3 through 6 present studies of longitudinal hadronic shower development utilizing the above parameterization. We have chosen to use the fitted constants of Ref. 3 because they are based on data with the widest range of incident energy hadrons, including the highest energy of 400 GeV, and because the resultant parameterization behaves sensibly up to an incident energy of at least 1 TeV. Shower shapes using the fitted constants of Ref. 3 are shown in Fig. 3 for typical energies. Figure 4 presents the fraction of incident energy accounted for by the electromagnetic term versus incident energy for the four sets of fitted constants of Refs. 3 through 6. (An absorption length of 22 cm and a radiation length of 0.8 cm have been assumed.) It can be seen that results derived from Refs. 4 and 5 show unrealistic behavior beyond 100 GeV. Reference 6 gives reasonable behavior, but is based on incident energies up to only 150 GeV. At present, the model does not include longitudinal fluctuations of the showers except for fluctuations in the starting point of the shower. In particular, it neglects the fluctuations in a shower initiated by a hadronic particle which produces a large number of π^0's at an early stage of its development. These kinds of effects are only averaged when using parameterizations. Figure 5 presents a comparison at an incident energy of 50 GeV on solid lead of our parameterization to the longitudinal shower shape generated by the Monte Carlo programs FLUKA87[7], CASIM[8], and MARS10[9].

The transverse hadronic shape is a function of both incident energy and depth along the shower. Appropriate detailed data from measurements are scarce, particularly for large lateral distances. We have therefore used the shower program FLUKA87 to characterize the lateral shapes. For a given longitudinal slice at depth z, the transverse shape is parameterized as either a piecewise function of two exponentials ($z < 2\lambda$) or a single exponential ($z > 2\lambda$). A table of these fitted exponential slope constants based on calculations at 6 energies (1, 20, 50, 100, 500, and 1000 GeV) is used to characterize the entire energy and depth dependence of the lateral spread. Interpolation was not used for different energies. The material dependence of the shape (for reasonable choices of material)is weak when distances are expressed in absorption lengths. Figure 6 shows some typical profiles from FLUKA87. It is known that FLUKA87 agrees well with data in the lateral region for which data exist[10].

2.3 Implementation in simulation

These parameterizations are then implemented in a fast detector simulation program. The GEANT3[11] package was used as the basic framework for description of the detector geometry. Detectors of arbitrary geometry and composition may then be studied. The typical shower simulation for a hadron incident upon a calorimeter is carried out using the following steps:

1. Choose shower start position from the distribution $e^{-z/\lambda}$.
2. Step through material with step size, $\Delta z \sim 0.1\lambda$, and at each longitudinal step position, z, divide the appropriate energy deposition ,

$$\Delta E = \int_{z-\Delta z/2}^{z+\Delta z/2} \frac{dE}{dz}\, dz \ ,$$

   into thirds and deposit each of the thirds at three different transverse and azimuthal positions according to the dE/dr distribution obtained from fits to FLUKA87 and a uniform azimuthal distribution. This choice gives a reasonable number of depositions and acceptable time for calculation. We have not looked at the sensitivity of all of the results to using more than three azimuthal and transverse points per step position.
3. The contribution to the overall resolution due to intrinsic effects such as the sampling or the e/π response are included by smearing the energy deposited by each incident particle, according to the parameterization

$$\frac{\sigma(E)}{E} = c_1 + \frac{c_2}{\sqrt{E}}$$

   where

$$E = \text{total energy deposited}$$
$$c_1, c_2 = \text{parameters characterizing response}$$

   An incident particle deposits energy E. A new total deposited energy, E_{new}, is chosen from a gaussian distribution of variance $\sigma^2(E)$ centered on E. The individual depositions which originally summed to E are rescaled to add to E_{new}.

3. Physics signals with high $p_\perp$ jets

3.1 Calorimeter thickness

The question of calorimeter thickness can be approached from the point of view of asking how many absorption lengths are needed to contain a given fraction of a single hadron's or a jet's incident energy or from the point of view of how many absorption lengths are needed to observe a physics signal. Given the parameterization of Section 2.2, the question of thickness to contain a fraction of a single hadron's or a jet's energy can be calculated. The point of shower initiation was chosen from the distribution $e^{-z/\lambda}$. The depth in absorption lengths versus incident particle energy to contain 95% or 99% of a single hadron's energy is presented in Fig. 7. These curves represent average shower containment. Figures 8 and 9 present histograms of calorimeter depth required to contain 95% and 99% respectively of detectable energy of average incident jet energies of 1.5, 3.5, and 5.5 TeV. Detectable energy means the jet energy less the energy of any muons or neutrinos. The histograms

represent the effects of fluctuations in jet composition. The jets were generated by the program PYTHIA [12]. Figure 8, for example, shows that seven absorption lengths will contain 95% of the jet's detectable energy for 95% of generated 1.5 TeV jets. Similarly, Fig. 9 shows that 11.4 absorption lengths will contain 99% of the jet's detectable energy for 99% of generated 3.5 TeV jets. One should note that these conclusions depend on the longitudinal shower parameterization. For example, if the fitted constants of Ref. 6 are used, the calorimeter depths required for containment will increase by one to two absorption lengths. Of the fitted constants of Refs. 3 through 6, those of Ref. 6 yields the greatest containment depth. However they are based on data up to only 150 GeV. It should also be noted that a radiation length to absorption length ratio of 0.036 has been assumed for these and subsequent thickness calculations. The results presented are very insensitive to this ratio.

The observation of a quark compositeness signal via hadronic jets requires the reconstruction of TeV scale jets [13]. In order to study how calorimeter thickness affects the observation of this signal, $p_\perp$ spectra of jets were generated simulating QCD and QCD plus a compositeness signal. The compositeness scale (Λ) was 15 TeV and constructive interference was assumed. In each case jet masses were reconstructed, varying the calorimeter thickness. Figure 10 shows the QCD plus compositeness signal with an infinite thickness calorimeter and calorimeters of 8 and 11 absorption lengths. Included in this calculation were energy resolutions of $0.15/\sqrt{E}$ and $0.50/\sqrt{E} + 0.02$ for the electromagnetic and hadronic portions respectively. Figure 10 shows little if any degradation of the signal even with a thickness of eight absorption lengths. This conclusion also holds for the QCD-only signal. This can be understood by the shallowness of the slopes of the $p_\perp$ distributions in comparison to the several percent of energy either lost or smeared. Indeed this same conclusion was reached in Ref. 13, when considering resolution only. Thus a calorimeter with a thickness of 8 absorption lengths seems sufficient to observe compositeness with hadronic jets. It should be noted that longitudinal shower fluctuations have not been included in these calculations and may change conclusions that do not depend only on average shower shape.

3.2 High $p_\perp$ W's and transverse segmentation and shower spreading

Reconstruction of a hadronically decaying $W^\pm$ or Z^0 may be important in some physics searches (such as a heavy Higgs search [14]). There have been a number of studies [15, 16] sometimes conflicting, of the effects of calorimeter granularity (size of $d\eta, d\phi$ bins) on W mass resolution. We have chosen to revisit this issue using as a "benchmark" the highest $p_\perp$ W's that might be produced at the SSC. The effects of the transverse segmentation of a calorimeter with tower geometry on the mass reconstruction of high $p_\perp$ $W's$ (> 500GeV) have been studied. In addition, the effects of transverse shower spreading have also been examined.

Our procedure is as follows:

1. Centrally produced and hadronically decaying W's with $p_\perp > 500$ GeV and $\theta_W > 30°$ are generated with PYTHIA v4.9.
2. Two arrays binned in pseudorapidity versus azimuth weighted by $E_\perp$ are filled, one using 4-vectors and the other using the earlier described detector simulation with the full shower parameterizations. Neutrinos and muons appear as lost energy. Figure 11 displays the two methods. Only particles from the W decay are used in the reconstruction as these may be "tagged" in the Monte Carlo. The basic detector is a cylinder with $r_{\text{inner}} = 180$ cm and $r_{\text{outer}} = 400$ cm and a half-length = 400 cm. The absorption length is 22 cm and radiation length is 0.8 cm. These correspond roughly to the parameters of the Large Solenoid Detector (LSD) model from the 1987 Berkeley SSC Detector Workshop [17]. Figure 12 shows the detector geometry used.
3. The parameters that are varied in this study are the segmentation, $d\eta$ and $d\phi$, r_{inner} and r_{outer} and the absorption (λ) and radiation (X_0) lengths.
4. From an array of $E_\perp$ values, the mass m_W is calculated as

$$m_W = \sqrt{\left(\sum_i E_i\right)^2 - \left(\sum_i \vec{p_i}\right)^2}$$

where E_i and $\vec{p_i}$ are determined by the energy and position of the ith cell. The position is assigned to the center of the cell. Clustering algorithms are not employed since only particles from the W are used. This is done to clarify detector induced vs. clustering algorithm induced effects.

We have studied the m_W distribution versus granularity for a number of different cases which are described below. We will subsequently call the binned 4-vector study "ideal" and the more realistic detector with Large Solenoid Detector geometry and fast shower simulation "LSD".

In addition, we have studied the impact on W mass resolution from the pileup of "minimum bias" events for some of the cases to be described. Our "minimum bias" sample consisted of a 50-50 mixture of ISAJET [18] minbias and low $p_\perp$ QCD jet events (> 5 GeV/c). The simplest case is for single bunch crossing pileup where the number of interactions is given by a poisson distribution with mean 1.5. This is ideal in the sense that it represents operating conditions for a calorimeter that has a resolving time less than the collider interbunch spacing time. In a more realistic case the total number of interactions is given by integrating over 7 bunch crossings corresponding roughly to a 100

ns integration time. If our simple mass reconstruction algorithm is used with no additional cuts, reconstruction of the W mass is severly degraded due to pileup. For this reason, two cuts were used in our study of pileup effects:

1. The contributions of cells with $E_\perp < (d\eta/0.05)(d\phi/0.05) \times 1$ GeV were eliminated.
2. Cells outside a cone around the W direction with radius $= 0.5$ in η and ϕ space were eliminated. NOTE: While this is not possible experimentally, the mean direction of hadron energy flow is usually not too far from this.

These two cuts were applied only for the cases concerning pileup effects.

The various cases studied were:

1. Ideal detector, perfect energy resolution.
2. (a) Ideal detector, smeared energies, $c_1 = 0.01$ (0.02), $c_2 = 0.15$ (0.50) for EM (hadronic) depositions.

   (b) $c_1 = 0.01$ (0.02), $c_2 = 0.30$ (1.00) for EM (hadronic) depositions.
3. LSD, perfect energy resolution, $X_0 = 0.8$ cm, $\lambda = 22$ cm, $r_{\text{inner}} = 160$ cm, $r_{\text{outer}} = 400$ cm, no magnetic field, no pileup.
4. (a) As in (3) but with smeared energies, $c_1 = 0.01$ (0.02), $c_2 = 0.15$ (0.50) for EM (hadronic) depositions.

   (b) As in (3) but with smeared energies, $c_1 = 0.01$ (0.02), $c_2 = 0.30$ (1.00) for EM (hadronic) depositions.
5. As in (3) but with $r_{\text{inner}} = 80$ cm.
6. As in (3) but with $X_0 = 0.37$ cm $\lambda = 12.3$ cm, $r_{\text{inner}} = 80$ cm. These parameters correspond roughly to that of a compact uranium-silicon calorimeter [19].
7. As in (3) but with a 2 Tesla magnetic field.
8. As in (3) but with single bunch pileup.
9. As in (3) but with 7 bunch pileup.

Cases 1, 2, 3 and 4, m_W and no pileup

Figures 13 and 14 show typical mass peaks and Fig. 15 shows the m_W rms resolution where resolution is defined as sigma for an m_W window between 60 and 120 GeV. This window was selected to reduce effects of low mass tails in the distribution due primarily to energy carried away by neutrinos. The resolution for the ideal calorimeter (binned 4-vectors) improves with finer segmentation until $d\eta = d\phi = 0.03$ and then flattens out with no further improvement, confirming earlier studies [15, 16]. The W mass resolution including the effects of shower spreading shows a weaker segmentation dependence. The effects of detector resolution have also been checked for reasonable values of energy resolution, $c_1 = 0.01$ (0.02), $c_2 = 0.15$ (0.50) for EM (hadronic). Energy resolution effects are a relatively small contribution to the W mass resolution. This is not unexpected for W's in this $p_\perp$ range, in which one anticipates that angular resolution will primarily determine mass resolution.

Table 1

W mass and rms resolution (using $60 < m_W < 120$ GeV window for calculation). Values in parentheses are the rms values. Typical errors for the rms values are about 1 GeV.

Case	Segmentation $d\eta$ $(= d\phi)$ 0.01	0.03	0.05	0.10
1	77.5 (5.5)	77.8 (5.6)	77.9 (6.4)	80.5 (9.5)
2(a)	77.1 (6.1)	77.9 (5.6)	77.9 (6.4)	80.4 (9.7)
2(b)	77.1 (6.1)	77.9 (5.6)	77.9 (6.4)	80.4 (9.7)
3	82.0 (9.0)	82.6 (9.4)	83.4 (9.2)	84.8 (11.1)
4(a)	82.3 (8.9)	82.6 (9.5)	83.2 (9.6)	84.8 (11.2)
4(b)	82.8 (8.9)	83.2 (9.0)	83.5 (9.8)	85.1 (11.5)
5	87.4 (11.8)	87.6 (11.7)	82.5 (13.1)	89.2 (12.6)
6	84.1 (10.0)	84.0 (10.0)	84.9 (10.7)	86.3 (11.8)
7	84.0 (9.9)	not run	84.7 (10.1)	not run
8	not run	not run	78.8 (8.3)	not run
9	81.9 (8.9)	79.6 (8.5)	79.0 (8.6)	not run

Cases 5 and 6 (m_W and detector size)

What happens if r_{inner} is changed to 80 cm and $\lambda = 12.3$ cm? This situation corresponds roughly to some of the most compact and dense of the calorimeters proposed thus far [19]. Figure 16 shows that the m_W resolution is still dominated (if not more so) by shower spreading.

Case 7, (m_W and a Magnetic Field) If a 2 Tesla magnetic field is used, the W mass resolution worsens slightly, as can be seen from the two "starburst" points in Fig. 16.

Cases 8 and 9 (m_W and event pileup)

We add in pileup events and apply the cell $E_\perp$ and cone cuts described earlier and try to reconstruct the W. As shown in Fig. 17, pile-up effects can be controlled using the above cuts in the sense that the resolution is not different to within statistics from the case where pileup is absent. For lower $p_\perp$ W's (> 150 GeV), however, the above algorithm is not useful since particles are dispersed over larger

regions and the cone must be enlarged. Clustering algorithms are then necessary. This has not yet been pursued.

Table 1 summarizes the various scenarios described above. In addition, we tabulate reconstruction efficiencies in Table 2, where the efficiency is defined as the fraction of the events falling in a mass window ±10 GeV around the peak.

Table 2

Fraction of events falling within ±10 GeV of the peak.

Case	Segmentation $\delta\eta$ $(= \delta\phi)$			
	0.01	0.03	0.05	0.10
1	0.63	0.63	0.64	0.55
2(a)	0.65	0.65	0.63	0.54
3	0.62	0.59	0.57	0.55
6	0.59	0.60	0.58	0.52
9	0.61	0.59	0.55	not run

4. Conclusions

We have studied two aspects of calorimeter requirements for detection of high $p_\perp$ jets at the SSC. Our studies of a possible quark compositeness signature, which will be manifested in the central rapidity region, indicate that a calorimeter depth of eight absorption lengths or more would be sufficient to detect a compositeness signature. Energy leakage from a calorimeter of this depth does not significantly perturb the shape of the jet $p_\perp$ spectrum. A similar conclusion [16] has been reached from studies of the mass resolution of high $p_\perp$ W decays to jets. Hence, in the central rapidity region at the SSC, calorimeter depths beyond eight absorption lengths must be justified on a basis other than energy containment, for example, hadronic punchthrough and muon detection.

We have studied the effects of calorimeter granularity and energy resolution on the mass resolution of W's with $p_\perp > 500$ GeV. We conclude that, for this $p_\perp$ range, intrinsic hadronic shower spreading has a significant impact on W mass resolution for a calorimeter inner radius/absorption length less than about eight. For a calorimeter with an absorption length of 20-25 cm (typical of uranium-liquid argon or compensating lead-scintillator) a calorimeter radius greater than 1.6 m is needed to take advantage of decreasing the calorimeter granularity ($\delta\eta = \delta\phi = 0.05$) to improve the W mass resolution. It may be possible to take advantage of finer calorimeter granularity at a smaller radius at the expense of reduced efficiency by employing clustering algorithms to select hadronic W decays with well separated jets [20]. We have not yet studied this possibility. For such high $p_\perp$ W's, the effect of pile-up of minimum bias events may be removed by requiring a minimum $E_\perp$ in the calorimeter cells used in the reconstruction of the W mass.

References

1. E. Longo *et al.*, Nucl. Instrum. Meth. **128** (1975) 283.
2. Bollini *et al.*, Nucl. Instrum. Meth. **171** (1980) 237.
3. R. K. Bock, T. Hansl-Kozanecka, and T. P. Shah, Nucl. Instrum. Meth. **186** (1981) 533.
4. S. Aronson *et al.*, Nucl. Instrum. Meth. **A269** (1988) 492-506.
5. E. Hughes, "Measurement of Hadronic and Electromagnetic Shower Development between 10 and 140 GeV by an Iron-Scintillator Calorimeter," unpublished CDHS Internal Report, (August 1986).
6. J. Freeman and A. Beretvas, *Physics of the Superconducting Supercollider*, ed. by R. Donaldson and J. Marx (Snowmass CO, 1986) 482.
7. P. A. Aarnio, A. Fassò, J. Lindgren, J. Ranft and G. R. Stevenson, "Enhancements to the FLUKA86 Program (FLUKA87)," CERN TIS-RP/190 (1987); see also P. A. Aarnio, A. Fassò, H-J. Möhring, J. Ranft and G. R. Stevenson, "FLUKA86 User's Guide," CERN TIS-RP/168 (1986).
8. A. Van Ginneken, Fermilab Report FN-272, Fermilab, Batavia, IL, USA (1975).
9. N. V. Mokhov, J. D. Cossairt. Nucl. Instrum. Methods, **A244**, 349 (1986); N. V. Mokhov, Soviet J. Particles and Nuclei, (Sept.-Oct. 1987), pp. 408-426.
10. N. V. Mokhov, Sov. J. Part. Nucl. **18** (Sept.–Oct. 1987) 5, and N. V. Mokhov, private communication.
11. R. Brun *et al.*, "GEANT3," CERN DD/EE/84-1 (Sept. 1987).
12. H. U. Bengtsson and T. Sjostrand, *Physics of the Superconducting Supercollider*, ed. by R. Donaldson and J. Marx (Snowmass CO, 1986) 311.
13. V. Barnes *et al.*, *Proc. of the Workshop on Experiments, Detectors, and Experimental Areas for the Supercollider*, ed. by R. Donaldson and M. G. D. Gilchriese, Berkeley CA July 7-17 (1987) 235.
14. R. N. Cahn *et al.*, *Proc. of the Workshop on Experiments, Detectors, and Experimental Areas for the Supercollider*, ed. by R. Donaldson and M. G. D. Gilchriese, Berkeley CA July 7-17 (1987) 20.
15. E. Fernandez *et al.*, *Proceedings of the 1984 Summer Study on the Design and Utilization of the Superconducting Super Collider*, Eds. R. Donaldson and J. Morfín, Snowmass, Colorado (1984) 107.
16. J. Freeman and C. Newman-Holmes, *Proc. of the Workshop on Experiments, Detectors, and Experimental Areas for the Supercollider*, ed. by R. Donaldson and M. G. D. Gilchriese, Berkeley CA July 7-17 (1987) 673.
17. G. G. Hanson, S. Mori, L. G. Pondrom, and H. H. Williams, *Proc. of the Workshop on Experiments, Detectors, and Experimental Areas for the Supercollider*, ed. by R. Donaldson and M. G. D. Gilchriese, Berkeley CA July 7-17 (1987) 340.
18. F. E. Paige and S. D. Protopopescu, *Physics of the Superconducting Supercollider*, ed. by R. Donaldson and J. Marx (Snowmass CO, 1986) 320.
19. J. Kirkby *et al.*, *Proc. of the Workshop on Experiments, Detectors, and Experimental Areas for the Supercollider*, ed. by R. Donaldson and M. G. D. Gilchriese, Berkeley CA July 7-17 (1987) 388.
20. C. Newman-Holmes and J. Freeman, Workshop on Detector Simulation for the SSC, Argonne National Laboratory Report ANL-HEP-CP-88-51 (1987) 285. See also Ref. 16.

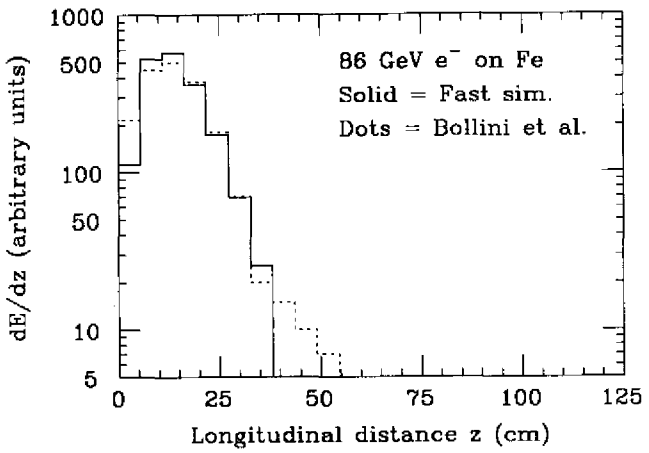

FIG. 1. A comparison of data from 86 GeV electrons incident on an iron calorimeter with our fast shower simulation. Energy deposition vs. longitudinal depth in shower.

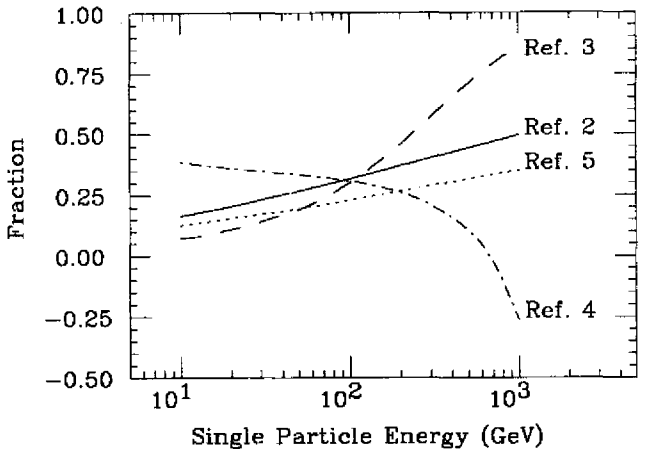

FIG. 4. Fraction of the incident energy accounted for by the electromagnetic term vs. incident energy using the parameterization given in the text and the fitted constants of Refs. 3 through 6.

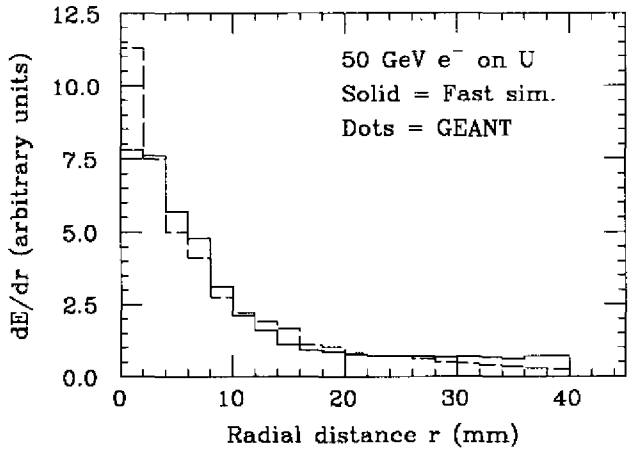

FIG. 2. A comparison of the radial electromagnetic shower shape for 50 GeV electrons on uranium from GEANT3 (solid histogram) and our parameterization (dashed histogram).

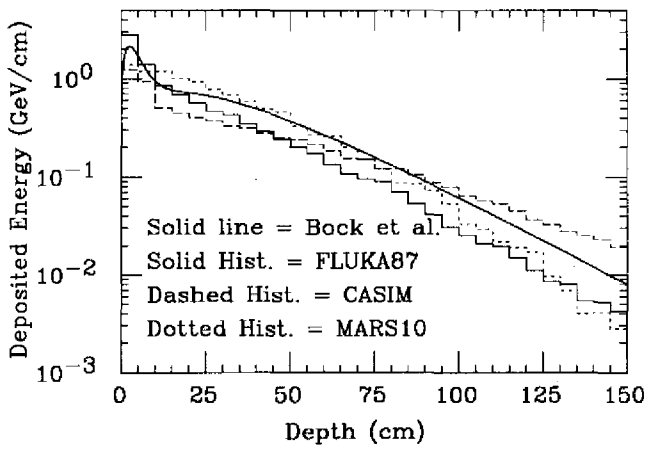

FIG. 5. A comparison of the longitudinal hadronic shower parameterization (Bock *et al.*) with three Monte Carlo programs (CASIM, FLUKA87, and MARS10) for 50 GeV hadrons incident on solid lead.

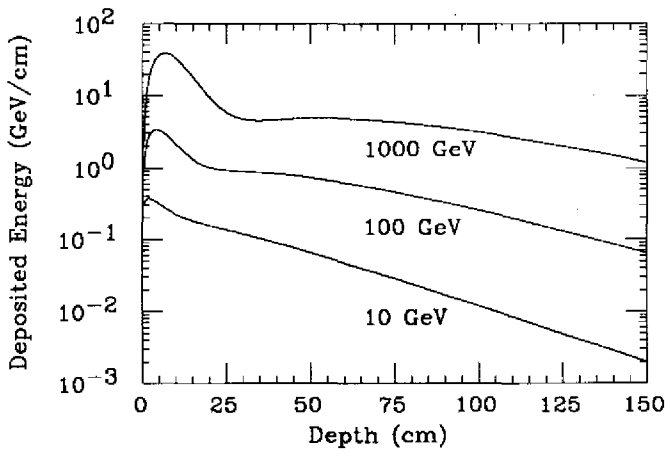

FIG. 3. The longitudinal hadronic shower shape for hadrons of several energies incident on a medium with an absorption length of 22 cm and a radiation length 0.8 cm, using the parameterization given in the text and the fitted constants of Ref. 6.

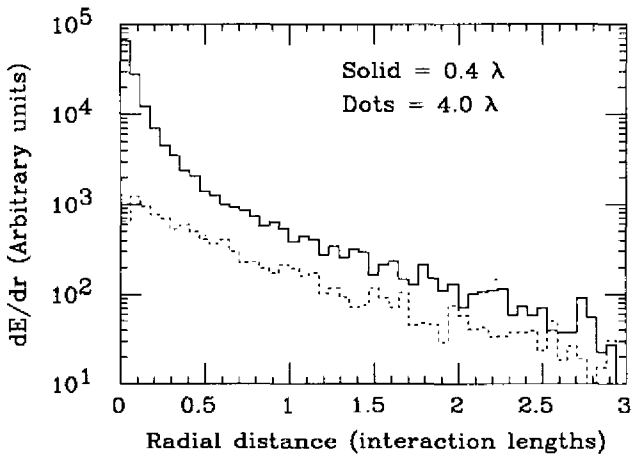

FIG. 6. Radial distributions as calculated by FLUKA87 (solid histogram) for 50 GeV incident hadrons at longitudinal depths of 0.4 λ and 4.0 λ.

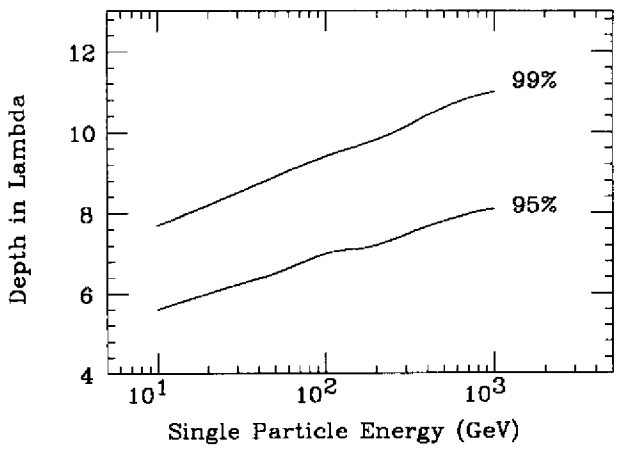

FIG. 7. The depth in absorption lengths vs. incident particle energy to contain 95% and 99% of a single hadron's energy, using the parameterization given in the text and the fitted constants of Ref. 4.

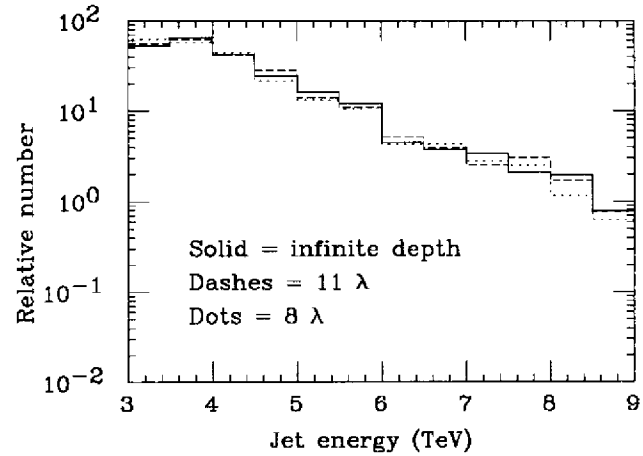

FIG. 10. The $E_\perp$ distribution of jets assuming a compositeness scale of 15 TeV with constructive interference for an infinite depth calorimeter and for calorimeter depths of 8 and 11 absorption lengths.

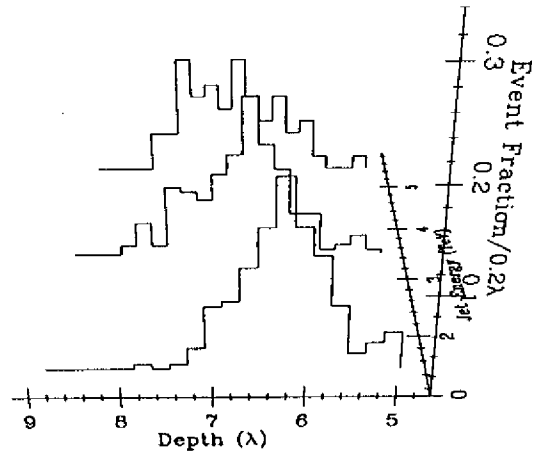

FIG. 8. Histograms of the fraction of jets vs. the number of absorption lengths to contain 95% of the jet's detectable energy for average jet energies of 1.5, 3.5, and 5.5 TeV. The histograms are normalized to unit area.

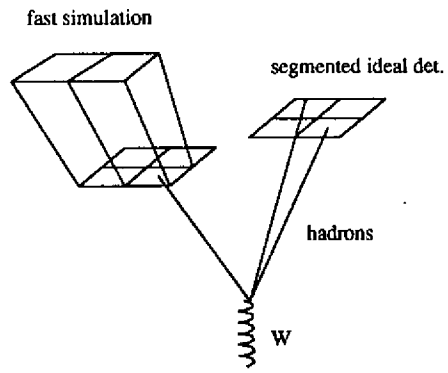

FIG. 11. A schematic representation showing the difference between an ideal detector and simulation with fast shower parameterization.

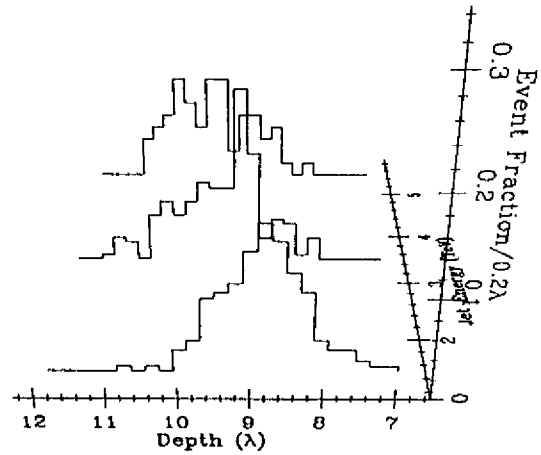

FIG. 9. Histograms of the fraction of jets vs. the number of absorption lengths to contain 99% of the jet's detectable energy for average jet energies of 1.5, 3.5, and 5.5 TeV. The histograms are normalized to unit area.

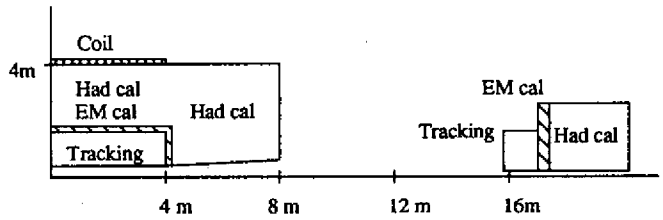

FIG. 12. Picture of the geometry assumed for simulations of a large solenoid detector.

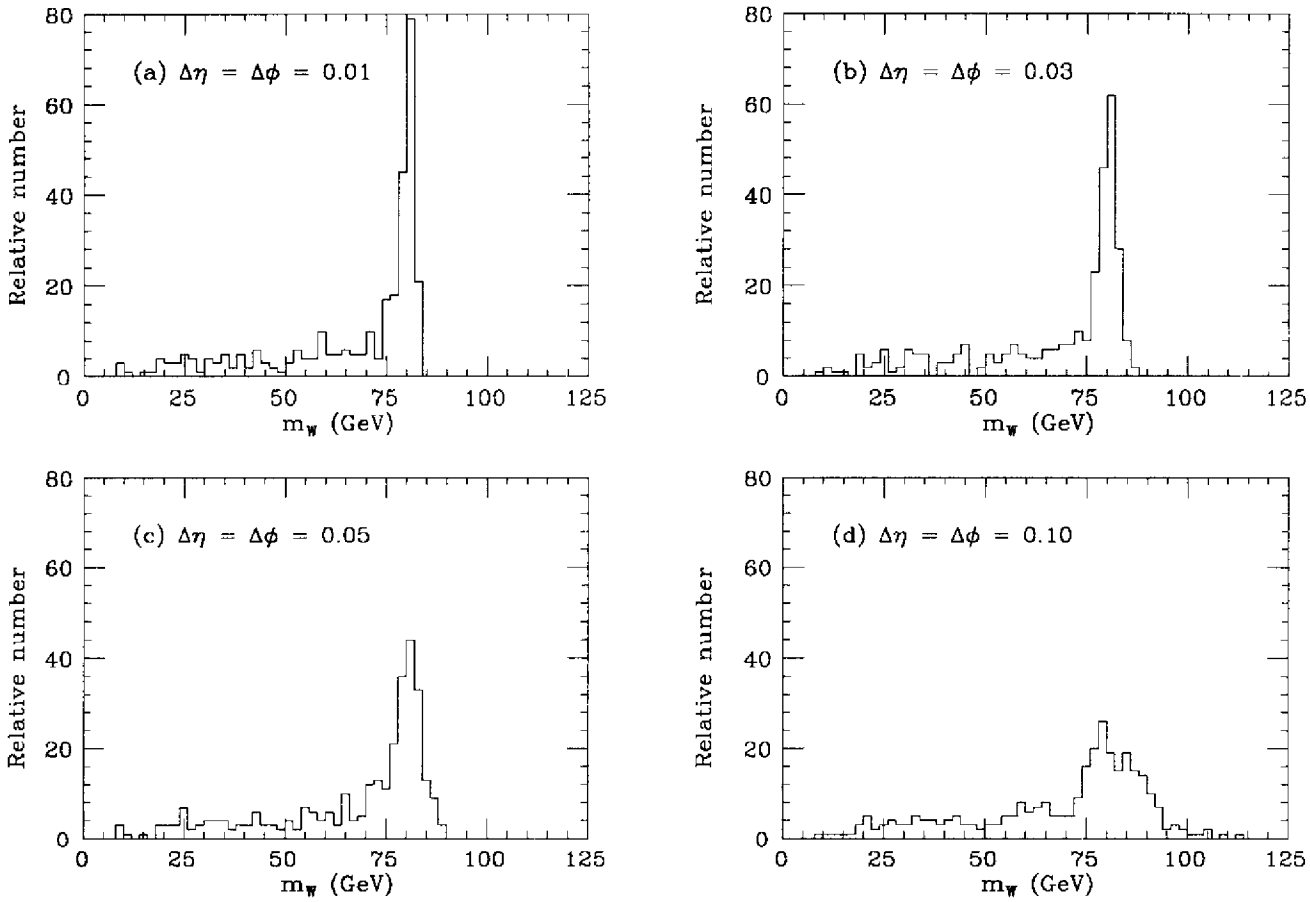

FIG. 13. Case 1: The W mass distribution assuming mass reconstruction using 4-vectors binned in rapidity and azimuth.

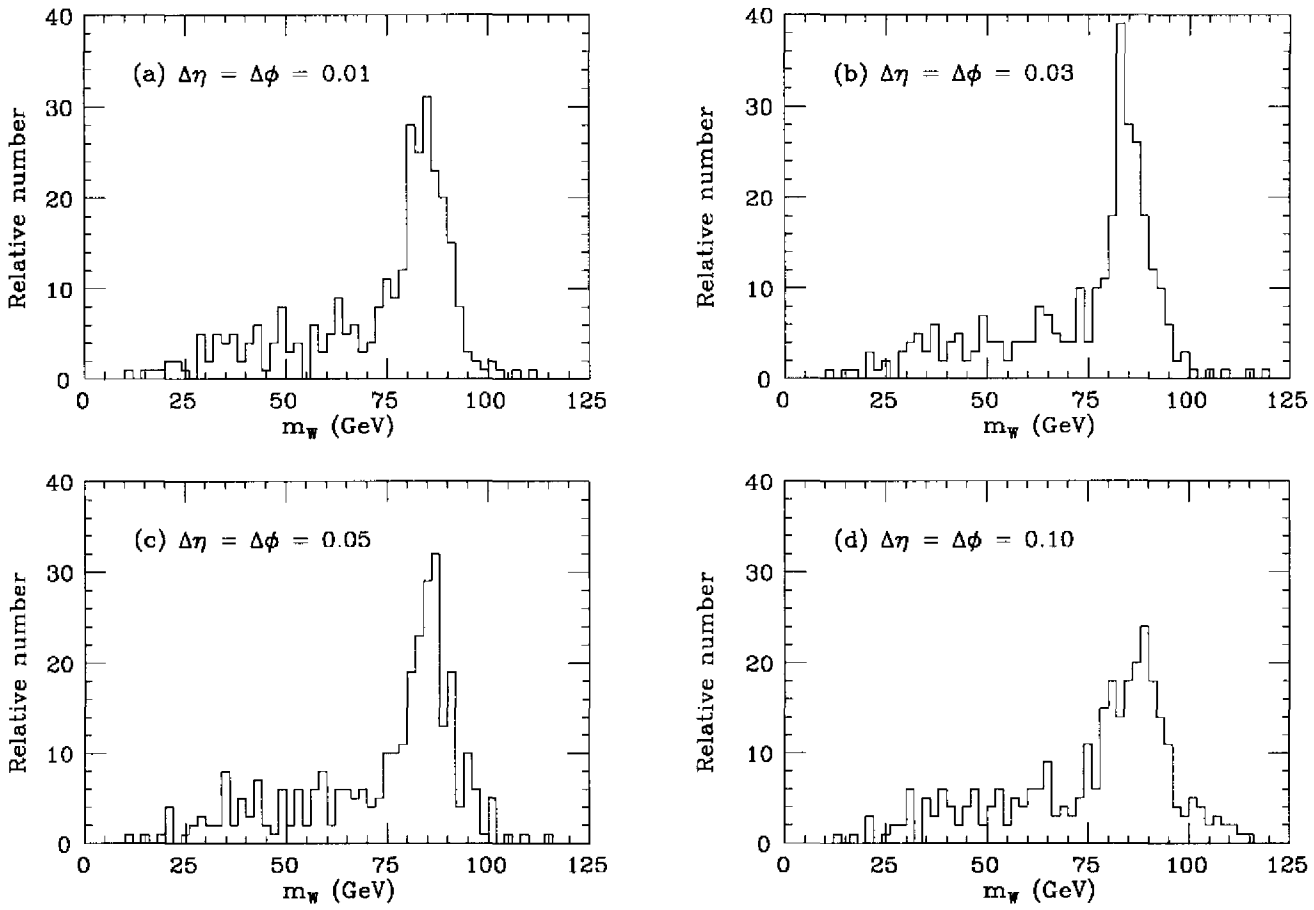

FIG. 14. Case 3: The W mass distribution with perfect energy resolution using the LSD detector simulation.

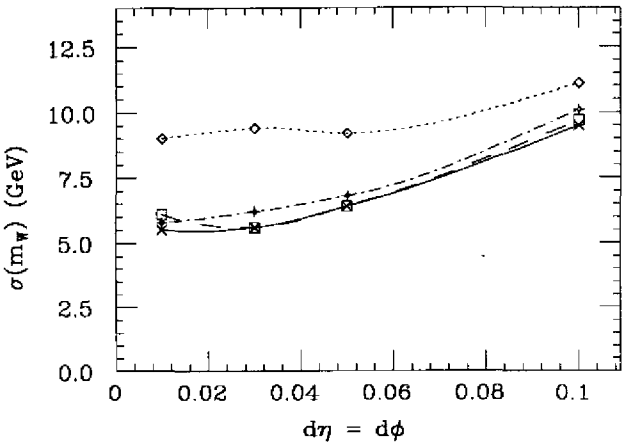

FIG. 15. The W mass resolution (as defined in the text) as a function of calorimeter segmentation ($\Delta\eta = \Delta\phi$) for the cases shown, as described in the text. No event pileup is present. Case 1 is shown as a solid curve, Case 2(a) as dashes, Case 2(b) as dot-dashes, and Case 3 as dots.

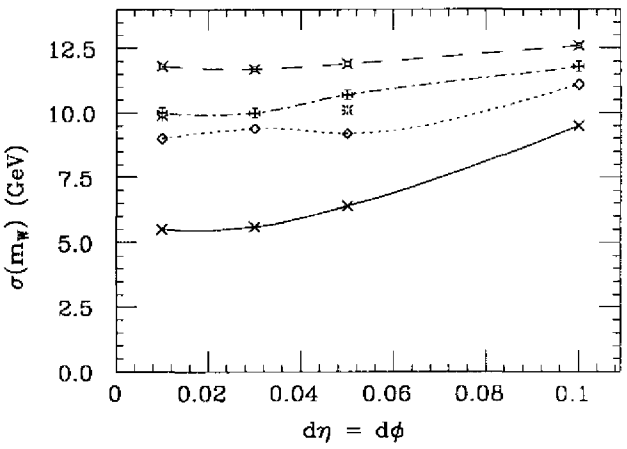

FIG. 16. The W mass resolution for different inner calorimeter radii and absorption lengths. For comparison, Case 1 is shown as solid, Case 3 as dots, Case 5 as dashes, Case 6 as dot-dashes and Case 7 as starburst points.

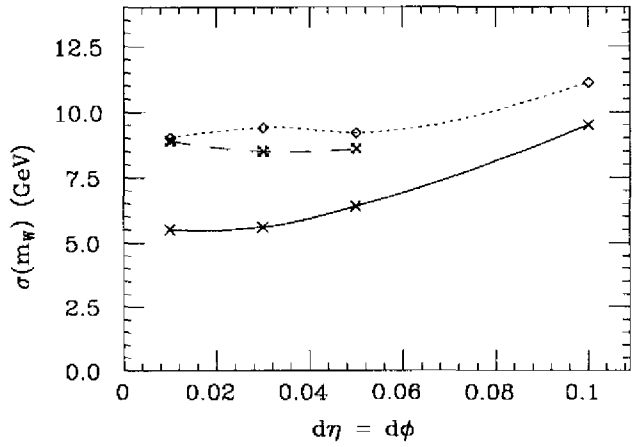

FIG. 17. The W mass resolution, including pileup as described in the text. Case 1 is shown as solid, Case 3 as dots and Case 9 as dashes.